Chemical Physics Letters 492 (2010) 276–280

Contents lists available at ScienceDirect

Chemical Physics Letters

journal homepage: www.elsevier.com/locate/cplett

The electrode potentials of the Group I alkali metals in the ionic liquid *N*-butyl-*N*-methylpyrrolidinium bis(trifluoromethylsulfonyl)imide

Rahmat Wibowo, Leigh Aldous, Sarah E. Ward Jones, Richard G. Compton *

Department of Chemistry, Physical and Theoretical Chemistry Laboratory, Oxford University, South Parks Road, Oxford OX1 3QZ, United Kingdom

ARTICLE INFO

Article history:
Received 8 April 2010
In final form 26 April 2010
Available online 4 May 2010

ABSTRACT

The redox couples M/M$^+$ of the Group I alkali metals Lithium, Sodium, Potassium, Rubidium and Caesium have been extensively investigated in a room temperature ionic liquid (IL) and compared for the first time. Cyclic voltammetric experiments in the IL *N*-butyl-*N*-methylpyrrolidinium bis(trifluoromethylsulfonyl)imide ([C$_4$mpyrr][NTf$_2$]) and subsequent simulation of the data has allowed the determination of the formal potential (E_f^0 vs. ferrocene/ferrocenium), standard electrochemical rate constant (k^0) and transfer coefficient (α) for each couple in the group. The trend in E_f^0 in [C$_4$mpyrr][NTf$_2$] is remarkably similar to the established trend in the common battery electrolyte, propylene carbonate.

1. Introduction

The Group I alkali metals, consisting of Lithium (Li), Sodium (Na), Potassium (K), Rubidium (Rb), Caesium (Cs) and Francium (Fr) are all extremely strong reducing agents, although their relative reducing ability depends upon which solvents they are in contact with. Their electrochemistry is of importance to a number of areas, most notably with respect to batteries and energy storage [1,2].

Ionic liquids (ILs) generally possess extremely low volatility and inherent conductivity, and can possess good chemical robustness, non-flammability (with respect to common organic solvents) and wide electrochemical windows, amongst other desirable properties [3,4]. The IL *N*-butyl-*N*-methylpyrrolidinium bis(trifluoromethylsulfonyl)imide ([C$_4$mpyrr][NTf$_2$]), possessing the above said properties, has allowed us the investigate the electrochemical redox properties of the first five Group I metals in a non-haloaluminate IL for the first time; by necessity the radioactive and extremely rare Francium had to be excluded.

We have previously reported in-depth studies on the behaviour of the Li/Li$^+$ [5,6] and Na/Na$^+$ [7] redox couple in a range of ILs at Platinum (Pt) and Nickel (Ni) microelectrodes. No evidence of alloy formation between the Group I metals and Ni was observed, while [C$_4$mpyrr][NTf$_2$] gave the most defined metal deposition and stripping processes, allowing accurate determination of fundamental parameters such as E_f^0, k^0 and α. In this study we complete the Group I series by investigating the K/K$^+$, Rb/Rb$^+$ and Cs/Cs$^+$ redox couples in [C$_4$mpyrr][NTf$_2$] at a Ni microelectrode. By focussing attention upon the reverse sweep of the CV, when the microelectrode has been electrodeposited with the Group I metal, the system behaves as an M/M$^+$ half-cell, yielding fundamental values that have been accurately referenced with respect to ferrocene/ferrocenium.

2. Experimental

2.1. Instruments and chemicals

The structure of *N*-butyl-*N*-methylpyrrolidinium bis(trifluoromethylsulfonyl)imide, [C$_4$mpyrr][NTf$_2$], is shown in Fig. 1, which was kindly donated by Merck KGaA. The alkali metal–[NTf$_2$]-salts were prepared by the reaction of aqueous solutions of the appropriate metal hydroxide salt with a 5% molar excess of H[NTf$_2$], followed by repeated dissolution in water then drying under vacuum, until pH neutral.

All electrochemical measurements were carried out using a computer-controlled μ-Autolab potentiostat (Eco-Chemie, Netherlands). Voltammetric measurements were conducted by applying a conventional two-electrode arrangement with a nickel microelectrode (50 μm diameter, fabricated in house as described previously [5–7]) used as a working electrode and a silver wire (Advent Research Materials Ltd., UK, 99.99%) served as a *quasi*-reference electrode. A section of a disposable micropipette tip (Eppendorf, Germany) was placed on the top of the working electrode, into which 20 μL of a [C$_4$mpyrr][NTf$_2$] solution containing 10 mM ferrocene and 0.1 M metal salt was added. The electrodes were confined in a T-shaped cell as described previously [8,9] and purged under a vacuum for 6 h prior to and during the experiments. This step is extremely important, as necessary to remove O$_2$ and H$_2$O, which will react with the alkali metal as well as reduce the electrochemical window of the IL [10–12].

In addition, 10 mM ferrocene (Fc) was introduced to every sample. This was used as an internal reference, and the formal

---

* Corresponding author. Fax: +44 (0) 1865 275 410.
E-mail address: richard.compton@chem.ox.ac.uk (R.G. Compton).

0009-2614/$ - see front matter © 2010 Elsevier B.V. All rights reserved.
doi:10.1016/j.cplett.2010.04.063

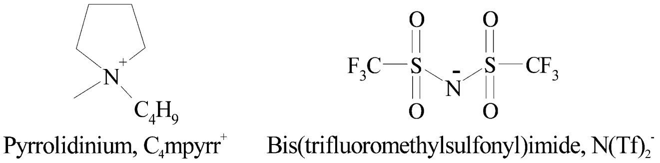

Fig. 1. The structure of $[C_4mpyrr][NTf_2]$.

potential of the Fc/Fc^+ redox couple (careful calculated after taking into account the discrepancies in diffusion coefficients between the two species, as described previously [7]) was set as 0 V.

2.2. Simulation conditions

The mathematical simulation model has been described [13] and applied [5–7,14,15] previously. Briefly, the model assumes a one electron transfer mechanism for the deposition and stripping of bulk alkali metal (M) on the electrode surface (Eq. (1)). Both the deposition and stripping processes are assumed to follow Butler–Volmer kinetics (Eqs. (2) and (3)).

$$\mathrm{M}^+_{(\mathrm{sol})} + e^- \underset{k_d}{\overset{k_a}{\rightleftharpoons}} \mathrm{M}_{(\mathrm{s})} \tag{1}$$

$$k_a = k^0 \exp\left(\frac{-\alpha F}{RT}(E - E_f^0)\right) \tag{2}$$

$$k_d = k^0[\mathrm{M}]^* \exp\left(\frac{(1-\alpha)F}{RT}(E - E_f^0)\right) \tag{3}$$

where k^0 is the surface process rate constant (units of $\mathrm{cm\,s^{-1}}$) for the M^+/M couple, α is the transfer coefficient and E_f^0 is the formal potential. $[M]^*$ is the standard concentration equal to $1 \times 10^{-3}\ \mathrm{mol\,cm^{-3}}$. R is the ideal gas constant ($8.314\ \mathrm{J\,K^{-1}\,mol^{-1}}$), F is the Faraday constant ($96\,485\ \mathrm{C\,mol^{-1}}$) and T is the absolute temperature in K.

Fick's second law is assumed to be followed for the diffusion process of species M^+ approaching and escaping the electrode surface. The surface coverage of M on the electrode, Γ_M, is dependant upon the rate of deposition and stripping. Deposition is M^+ concentration dependant; therefore the concentration gradient had to be solved using a series of partial differential equations, as described previously [13]. The maximum distance simulated is set to be $6\sqrt{Dt}$ from the electrode surface, where D is the diffusion coefficient of M^+ and t is time. It is considered that there is no concentration gradient beyond that distance. The rate of stripping is assumed to be independent of Γ_M.

After the system of equations has been solved, the current, I, was calculated using the following equation:

$$I = -2\pi F \int_0^{r_d} \frac{\partial \Gamma_{\mathrm{Li}}}{\partial t} r\,dr. \tag{4}$$

3. Results and discussion

3.1. Voltammetric results

Fig. 2 displays a comparison of CVs for all five Group I alkali metals, recorded for 0.1 M of the relevant metals–$[NTf_2]$-salt dissolved in $[C_4mpyrr][NTf_2]$ and recorded at $10\ \mathrm{mV\,s^{-1}}$ at a Ni microelectrode.

Underpotential deposition (UPD) processes [5–7] were observed for all five Group I metals in the region of −2 to −3 V, and can be observed most clearly in Fig. 2 for Li^+. Relatively sharp reduction profiles were observed for all metals at potentials more negative than −3 V, consistent with an overpotential being required for the initial nucleation of the Group I metal to occur on Ni, followed by the rapid deposition of metal-on-metal. The local concentration of the metal ion is therefore depleted, and in the case of Li^+, Na^+ and K^+ this leads to a characteristic peak shape corresponding to a mass transport controlled region [16]. All scans also possess characteristic nucleation loops (where backward and forward currents cross over), as on the reverse scan Group I metal is still being deposited on Group I metal at potentials positive to that required for the initial nucleation of the metal on Ni. In the case of Rb^+ and Cs^+, the reduction potentials for these metals were significantly more negative than that of Li^+, Na^+ and K^+, such that nucleation occurred only a few millivolts prior the reduction process of $[C_4mpyrr][NTf_2]$. Therefore the scan had to be reversed shortly after nucleation, and a considerable amount of metal was instead deposited on the reverse scan (direction of the scan indicated by arrows in the figure).

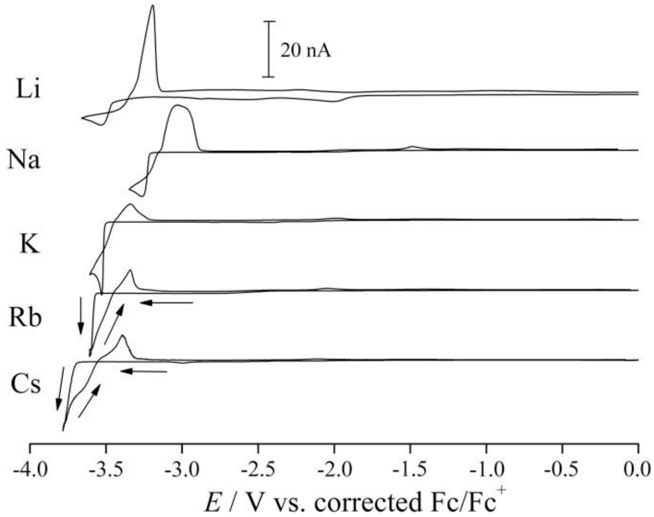

Fig. 2. The cyclic voltammograms recorded for a 0.1 M solution of the relevant metal–$[NTf_2]$ salt in $[C_4mpyrr][NTf_2]$ at a 50 μm diameter Ni electrode. Scan rate = $10\ \mathrm{mV\,s^{-1}}$.

The charge passed under the reduction process can be used to quantify the amount of alkali metal reduced at the electrode surface. Assuming the metal is deposited as layers with the same geometric area as that of the Ni microelectrode, the reduction charge calculated for the bulk reduction peak in the voltammograms in Fig. 2 indicates that approximately 63, 96, 34, 33 and 68 layers of Li, Na, K, Rb and Cs were deposited, demonstrating that all systems deposit bulk metal on the Ni electrode. All systems also display sharp oxidation peaks which correspond to the stripping off of metal from the electrode surface. Therefore, the CV response after the bulk deposition peak and prior to the bulk stripping peak (e.g. where the CV crosses over the x-axis, corresponding to zero net current being passed) corresponds to the system behaving as an M/M^+ interface, as opposed to Ni/M^+. The response of the system in this region is therefore a feature of the fundamental parameters of the M/M^+ couple in the IL. The CVs were simulated as described below in order to quantify the parameters.

3.2. Simulation results

The details of the simulation were explained briefly in Section 2. Full details of the development of the simulation model [13], as well as its application to experimental results have been previously demonstrated [5–7,14,15]. The simulation model was applied to the K/K^+, Rb/Rb^+ and Cs/Cs^+ systems in order to extract the fundamental electrochemical parameters of the couples. Figs. 3–5 display overlays of the experimental results as well as best fits for

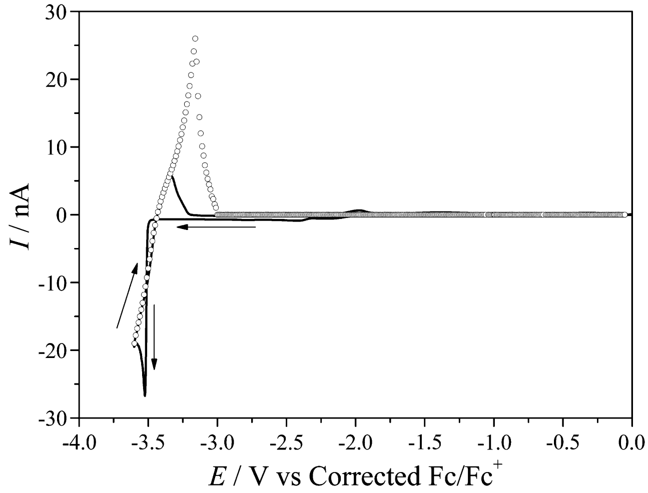

Fig. 3. The fit of the experimental (–) and simulation (○) data for the cyclic voltammetry experiment using 0.1 M K[NTf$_2$] in [C$_4$mpyrr][NTf$_2$] on a 50 μm diameter Ni electrode. Scan rate = 10 mV s^{-1}.

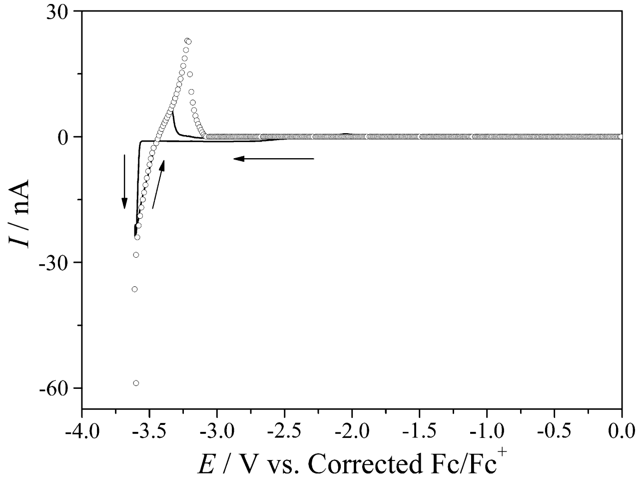

Fig. 4. The best fit of experimental (–) and simulation (○) data for the CV of 0.1 M Rb[NTf$_2$] in [C$_4$mpyrr][NTf$_2$] on 50 μm diameter Ni electrode. Scan rate = 10 mV s^{-1}.

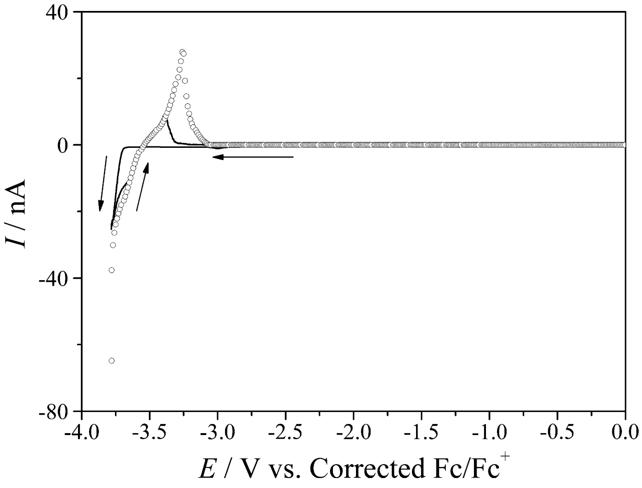

Fig. 5. The best fit of experimental (–) and simulation (○) data for the CV of 0.1 M Cs[NTf$_2$] in [C$_4$mpyrr][NTf$_2$] on 50 μm diameter Ni electrode. Scan rate = 10 mV s^{-1}.

the simulations for K/K$^+$, Rb/Rb$^+$ and Cs/Cs$^+$, respectively. The simulation of the Li/Li$^+$ [5] and Na/Na$^+$ [7] systems has been reported previously.

The simulation can be split into three areas; the alkali metal deposition peak, the alkali metal stripping peak, and the region of zero current in between the two processes.

The simulated alkali metal ion deposition peaks do not precisely match the experimental results, as shown in Figs. 3–5. This is because the simulated results do not take into account the nucleation process, replication of which is not required for an investigation of solely M/M$^+$ parameters. The simulation was started in the region where initial nucleation was observed to occur in the experimental results. The physical parameters were put into the simulations, and the amount of metal deposited was solved. By varying the parameters a good fit could be achieved on the reverse scan, which also resulted in the simulation generating the appropriate concentration gradient for M$^+$ extending out from the electrode surface required for a good fit during the zero current cross-over region (occurring *ca.* 30 s after deposition is started).

As the shape of the reduction peak after the initial nucleation process is mass transfer controlled, it is also extremely sensitive to the diffusion coefficient, *D*, of the ion M$^+$. Fitting to the experimental reduction process for K$^+$ (as shown in Fig. 3) was used to accurately determine *D*. The *D* for Li$^+$ [5] and Na$^+$ [7] have been previously reported. However, since clear mass transfer controlled regions could not be observed in the case of Rb/Rb$^+$ and Cs/Cs$^+$, the diffusion coefficient could not be independently determined. The *D* values for Li$^+$, Na$^+$ and K$^+$ were found to be linear with respect to $1/r$, where *r* is the radius of the ion. This allowed us to extrapolate the trend and estimate *D* values for Rb$^+$ and Cs$^+$ based upon their known *r* values. These estimated *D* values were found to work well in the subsequent simulations.

For all of the metals the simulation displays stripping peaks significantly higher than that of the experimental result, as the simulation assumes 100% stripping efficiency. However, the foot of the stripping peak fitted well in all cases, indicating that during the reverse scan bulk alkali metal was present on the surface of the electrode. Therefore, in the potentials between bulk deposition and bulk stripping, the electrode is behaving as an alkali metal electrode, M, in contact with a precisely defined local concentration of its ion, M$^+$. The current in the cross-over region area (*ca.* ±100 mV from the *x*-axis cross-over potential) is a function of both oxidation and reduction processes occurring appreciably at the M/M$^+$ interface, as defined by Butler–Volmer kinetics (see Section 2 for more details) and is therefore sufficiently sensitive to E_f^0, α and k^0 for these values to be determined accurately by focussing on the simulation of this region. The values of E_f^0, α and k^0 were therefore varied until the best fit was obtained between simulation and experimental results for the tail end of metal deposition, the cross-over region and the foot of the oxidation peak. The good fit obtained between experimental and simulation data is clearly observed in Figs. 3–5.

Table 1 presents the electrochemical parameters which include diffusion coefficient (*D*), electrochemical rate constant (k^0), formal potential (E_f^0), and transfer coefficient (α) required for the best fits shown in Figs. 3–5. The data for the Li/Li$^+$ [5] and Na/Na$^+$ [7] redox couples are those published previously.

From Table 1 the increase in diffusion coefficient (*D*) down the group can clearly be observed for Li$^+$, Na$^+$, and K$^+$. It should be recalled that D was estimated for Rb$^+$ and Cs$^+$. Similar trends down Group I have previously been observed in aqueous [17,18] and methanol solutions [19]. The electrochemical rate constant (k^0) was also found to decrease slightly down the group. The transfer coefficients are all above 0.5 implying a late transition state, presumably due to the M$^+$ ion being largely desolvated. The formal potential (E_f^0) displays a similar trend to that reported for a variety of

Table 1
The electrochemical parameters for the alkali metal redox couples in [C_4myprr][NTf_2], extracted by simulation of the experimental data, where D is the diffusion coefficient, k^0 is the standard electrochemical rate constants, E_f^0 is the formal potential, α is the transfer coefficient and ΔG^0_{solv} is the Gibbs energy of solvation in H_2O or [C_4myprr][NTf_2].

M/M^+	10^8D ($cm^2\ s^{-1}$)	10^5k^0 ($cm\ s^{-1}$)	E_f^0 (V vs. corrected Fc/Fc^+)	α	$\Delta G^0_{solv(H_2O)}$ ($kJ\ mol^{-1}$)[c]	$\Delta G^0_{solv(IL)}$ vs. Fc/Fc^+ ($kJ\ mol^{-1}$)
Li/Li^+[a]	4.5 ± 0.1	1.20 ± 0.05	−3.250 ± 0.010	0.63 ± 0.01	−509	−336 ± 10
Na/Na^+[a]	7.8 ± 0.4	1.15 ± 0.06	−3.066 ± 0.003	0.63 ± 0.02	−409	−278 ± 10
K/K^+	10.2 ± 0.5	0.3 ± 0.05	−3.359 ± 0.005	0.80 ± 0.05	−335	−157 ± 10
Rb/Rb^+	10.9 ± 0.5[b]	0.3 ± 0.04	−3.367 ± 0.003	0.75 ± 0.05	−314	−132 ± 10
Cs/Cs^+	11.5 ± 0.5[b]	0.2 ± 0.05	−3.472 ± 0.003	0.75 ± 0.05	−283	−86 ± 10

[a] The data for Li/Li^+ and Na/Na^+ are taken from Refs. [5,7], respectively.
[b] D values estimated by extrapolation from a plot of Li^+, Na^+ and K^+ D values vs. $1/r$, where r is the ionic radii.
[c] $\Delta G^0_{solv(H_2O)}$ values from reference [26].

other solvents (discussed below). In Table 1 E_f^0 is reported vs. Fc/Fc^+, where the formal potential of Fc/Fc^+ has been carefully corrected with respect to the discrepancies in diffusion coefficients that can arise between redox couples in ILs [20], and this correction method has been described previously [7].

The trend in formal potential of the metal redox couples has been reported for a number of solvents [21]. However, quantitative comparison is made difficult by the lack of a rigorous reference potential for ILs [15,20,22]. While extensive work aimed primarily at Lithium and energy storage applications has been reported in ILs [23–25], few quantitative values have been published that can be compared with. Wilkes et al. carried out a study aimed at the reduction potentials of the alkali metals in a neutral, buffered [C_2mim]Cl:$AlCl_3$ melt, although this was limited to the reduction potentials for amalgam formation at a Hg-film electrode, due to the electrochemical window of the melt not supporting deposition of the pure metal [26].

Fig. 6 displays a comparison of the trends in E_f^0 for the Group I metals relative to the E_f^0 of the Li/Li^+ couple in the same medium. It can be observed that the trend in formal potential in H_2O, DMSO and DMF [21], going from most positive to negative, is Na > K > Rb > Cs > Li. In the case of amalgam formation potentials in [C_2mim]Cl:$AlCl_3$ [26], the trend goes down the group, such that Li > Na > K > Rb > Cs. In [C_4mpyrr][NTf_2] the trend in E_f^0 displays a remarkable similarity to propylene carbonate, with Na > Li > K ≈ Rb > Cs.

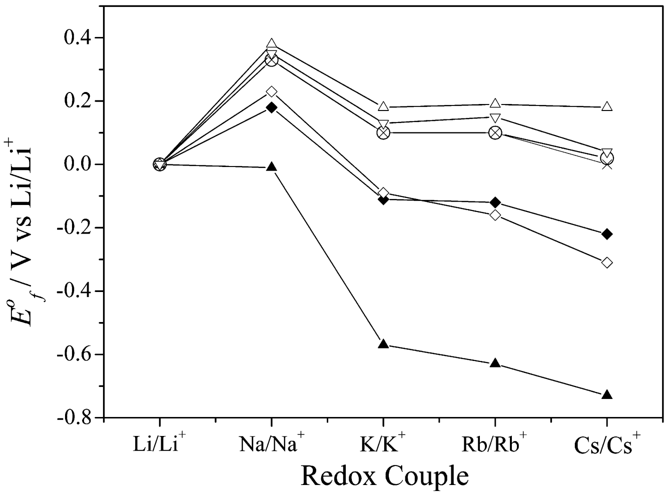

Fig. 6. The plot of alkali metal redox couple formal potential relative to the Li/Li^+ couple in (△) 60% DMSO/40% H_2O (▽) DMSO, (○) H_2O, (×) DMF, (◇) propylene carbonate, (◆) [C_4mpyrr][NTf_2] (this work) and (▲) neutral, buffered [C_4mim]-Cl:$AlCl_3$ melt, at a Hg-film electrode (from Ref. [26]). All values with hollow symbols taken from Ref. [21].

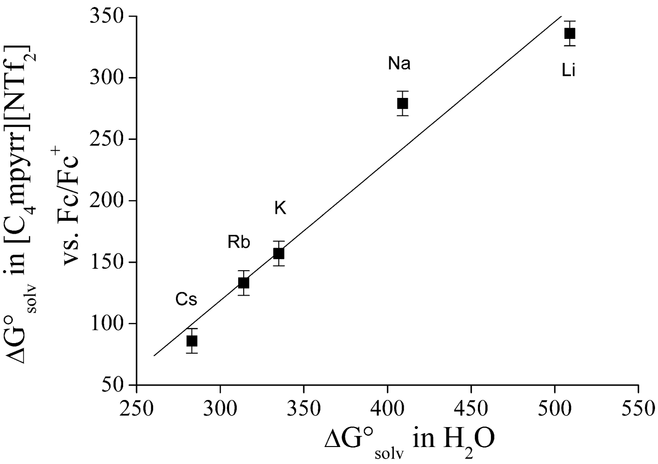

Fig. 7. The plot of the estimated Gibbs energy of solvation of the alkali metal ions in [C_4mpyrr][NTf_2] against the known Gibbs energy of solvation for the ions in aqueous solution.

The trend in solvation energy can be estimated by using the obtained E_f^0 values. A Born–Haber cycle can be used to calculate the Gibbs energy of solvation, ΔG^0_{solv}, by comparison with the known values for the Gibbs energy of ionisation and sublimation, as well as the single-electrode reduction potential [26]. Lacking a reliable single-electrode reference potential for [C_4mpyrr][NTf_2], as well as knowledge of activity coefficients in the IL environment, the relative solvation energies can nevertheless be estimated vs. Fc/Fc^+ by using the obtained E_f^0 vs. Fc/Fc^+ values for the alkali metals and assuming $E_f^0 = E^0$. Table 1 displays the calculated $\Delta G^0_{solv(IL)}$ vs. Fc/Fc^+ for the metals in [C_4mpyrr][NTf_2], as well as the literature values for $\Delta G^0_{solv(H_2O)}$ as comparison. Fig. 7 displays a plot of $\Delta G^0_{solv(IL)}$ vs. Fc/Fc^+ against $\Delta G^0_{solv(H_2O)}$, which indicates that the smaller ions are the most strongly solvated in both systems. A line of best linear fit has been included in order to guide the eye. However, it should be noted that a perfect linear fit would not be expected unless solvation behaviour is identical for the Group I ions in both H_2O and [C_4mpyrr][NTf_2].

4. Conclusions

In summary, the deposition and dissolution of all five Group I alkali metal redox couples (M/M^+) have been investigated in the ionic liquid *N*-butyl-*N*-methylpyrrolidinium bis(trifluoromethylsulfonyl)imide ([C_4mpyrr][NTf_2]) using a Ni microelectrode. All systems displayed chemically reversible behaviour which was successfully simulated using a mathematical model and the electrochemical rate constant (k^0), formal potential (E_f^0) transfer coefficient (α) and diffusion coefficient (D) have been extracted by simulation of the CV. This constitutes the first electrochemical investigation of an entire group in an ionic liquid. The reducing powers of the alkali metals in [C_4mpyrr][NTf_2] follow the trend previously observed for propylene carbonate, with Na > Li > K ≈ Rb > Cs.

Acknowledgements

R.W. thanks the Directorate of Higher Education, The Ministry of National Education, Republic of Indonesia for funding.

References

[1] M. Armand, F. Endres, D.R. MacFarlane, H. Ohno, B. Scrosati, Nat. Mater. 8 (2009) 621.
[2] J.F. Wishart, Energy Environ. Sci. 2 (2009) 956.
[3] D.S. Silvester, R.G. Compton, Z. Phys. Chem. 220 (2006) 1247.
[4] H.T. Liu, Y. Liu, J.H. Li, Phys. Chem. Chem. Phys. 12 (2010) 1685.
[5] R. Wibowo, S.E.W. Jones, R.G. Compton, J. Phys. Chem. B 113 (2009) 12293.
[6] R. Wibowo, S.E.W. Jones, R.G. Compton, J. Chem. Eng. Data 55 (2010) 1374.
[7] R. Wibowo, L. Aldous, E.I. Rogers, S.E.W. Jones, R.G. Compton, J. Phys. Chem. C 114 (2010) 3618.
[8] R.G. Evans, O.V. Klymenko, P.D. Price, S.G. Davies, C. Hardacre, R.G. Compton, ChemPhysChem 6 (2005) 526.
[9] U. Schroder et al., New J. Chem. 24 (2000) 1009.
[10] M.C. Buzzeo, C. Hardacre, R.G. Compton, ChemPhysChem 7 (2006) 176.
[11] A.M. O'Mahony, D.S. Silvester, L. Aldous, C. Hardacre, R.G. Compton, J. Chem. Eng. Data 53 (2008) 2884.
[12] E.I. Rogers, X.J. Huang, E.J.F. Dickinson, C. Hardacre, R.G. Compton, J. Phys. Chem. C 113 (2009) 17811.
[13] S.E.W. Jones, F.G. Chevallier, C.A. Paddon, R.G. Compton, Anal. Chem. 79 (2007) 4110.
[14] C.A. Paddon, S.E.W. Jones, F.L. Bhatti, T.J. Donohoe, R.G. Compton, J. Phys. Org. Chem. 20 (2007) 677.
[15] E.I. Rogers et al., J. Phys. Chem. C 111 (2007) 13957.
[16] R.G. Compton, C.E. Banks, Understanding Voltammetry, World Scientific Publishing, Singapore, 2007.
[17] H.S. Harned, M. Blander, C.L. Hildreth, J. Am. Chem. Soc. 76 (1954) 4219.
[18] D.G. Leaist, J. Goldik, J. Soln. Chem. 30 (2001) 103.
[19] S. Chowdhuri, A. Chandra, J. Chem. Phys. 124 (2006).
[20] E.L. Rogers, D.S. Silvester, D.L. Poole, L. Aldous, C. Hardacre, R.G. Compton, J. Phys. Chem. C 112 (2008) 2729.
[21] Y. Marcus, Pure Appl. Chem. 57 (1985) 1129.
[22] D.S. Silvester, E.I. Rogers, R.G. Compton, Reference electrodes for use in room temperature ionic liquids, in: F. Endres, A.P. Abbott, D.R. MacFarlane (Eds.), Electrodeposition from Ionic Liquids, Wiley-VCH, Weinheim, 2008, pp. 296–309.
[23] P.C. Howlett, D.R. MacFarlane, A.F. Hollenkamp, Electrochem. Solid State Lett. 7 (2004) A97.
[24] Y. Katayama, T. Morita, M. Yamagata, T. Miura, Electrochemistry 71 (2003) 1033.
[25] F. Endres, S.Z. El Abedin, N. Borissenko, Z. Phys. Chem. 220 (2006) 1377.
[26] C. Scordiliskelley, J. Fuller, R.T. Carlin, J.S. Wilkes, J. Electrochem. Soc. 139 (1992) 694.